Supporting Online Material for

The Primitive Wrist of *Homo floresiensis* and Its Implications for Hominin Evolution

Matthew W. Tocheri,* Caley M. Orr, Susan G. Larson, Thomas Sutikna, Jatmiko, E. Wahyu Saptomo, Rokus Awe Due, Tony Djubiantono, Michael J. Morwood, William L. Jungers

*To whom correspondence should be addressed. E-mail: tocherim@si.edu

Published 21 September 2007, *Science* **317**, 1743 (2007)
DOI: 10.1126/science.1147143

This PDF file includes:

SOM Text
Fig. S1
Tables S1 to S11
References

1 Materials and methods

The taxonomic breakdown of the total sample is shown in Table S1 while the geographic breakdown of the modern human sample is shown in Table S2. The wrist bones of the extant genera along with high-quality casts of all fossil specimens (except Shanidar 3 for which the original was available) were each laser scanned and modeled as a triangular mesh for analysis (Tables S1 and S2). The articular and nonarticular areas on each 3D bone model were digitally segmented using Raindrop Geomagic Studio 8 (software provided by the Partnership for Research In Spatial Modeling [PRISM] at Arizona State University). The segmentation process was generally performed while referring visually to the actual bone or cast. Subsequently, the relative areas of each articular surface and the angles between joint surfaces were quantified (*S1–S3*).

Absolute surface areas were calculated by summing the areas of all triangles in each desired region. In order to compare the articular and nonarticular areas of the differently sized genera, shape ratios were calculated that remove the effects of scale. These shape ratios are the proportion (%) of total bone surface area that is represented by each specific joint surface or nonarticular region. In other words, these ratios are scale-free shape variables and enable the examination of whether significant differences in shape exist between taxa (*S4, S5*).

Using principal components analysis on all the vertices of a given surface, the eigenvector associated with the smallest eigenvalue is the normal vector of the least-squares plane. The normal vectors of any two planes were used to compute the angle between the planes. The angle was calculated as 180° minus the inverse cosine (i.e., arccos) of the dot product of the normal vectors (*S1*). The angle between any two normal

vectors and hence, their respective planes, is always measured such that the two vectors occur in the same plane. Thus, the angles that are measured are independent of the orientation of the bone model.

Standard multivariate statistical techniques were used to analyze the 3D shape variables. Canonical variates analysis was used to reduce and graphically interpret the observed multivariate variation (*S6*). The resulting canonical variables were interpreted using the pooled-within canonical structure, which represents the correlations between pairs of linear combinations of the variables for each genus and each canonical variable. Discriminant analysis was used to estimate the posterior probability of belonging to a genus given a combined set of data values. The posterior probability represents the likelihood of correctly assigning an individual bone to its respective genus based on its 3D data values (i.e., shape). The cross-validation method was used to calculate the posterior probability of membership in each genus because it gives approximately unbiased estimates of the probabilities of misclassification (*S6*).

2 Archaeology of LB1

Initial recovery of the LB1 skeleton occurred in Sector VII of the September 2003 archaeological excavations (*S7, S8*). Sector VII is a 2 m by 2 m square, which was first excavated to a depth of 7.2 m (*S8*). The majority of skeletal elements assigned to LB1 were recovered *in situ* from hardened blocks of sediment from the south-east corner of Sector VII within Spit No. 59, which was between 5.8 m and 5.9 m below the surface of the cave (Fig. S1) (*S7, S8*). Wet sieving of sediments from this corner helped recover a few additional smaller elements. In total, over 50 non-duplicated hominin skeletal elements were found in Spit No. 59 (Table S3), with many of the lower postcranial

elements still in articulation with one another (*S7, S8*). The hand bones, which include the three wrist bones analyzed here, were recovered from the area within Sector VII immediately south of the cranium, between the cranium and the south baulk of the excavation (Fig. S1).

Subsequent excavations of Sector VII in 2004 continued to a depth of 11 m while an additional 2 m by 2 m square (Sector XI) was excavated immediately south of the initial square (*S9*). Together, these two adjoining squares resulted in a 2 m by 4 m area referred to as the Sector VII/XI trench (*S9*). Within Spit No. 58A (depth 5.7 m to 5.8 m) of Sector XI, additional skeletal elements were recovered immediately adjacent to Sector VII (Fig. S1). These included a right humerus, both ulnae, and a left fibula, all of which were assigned to LB1 because of their close stratigraphic association within Layer R to the remains found in Spit No. 59 of Sector VII, the lack of duplication of previously discovered elements, and the overall similarity in size and preservation (*S9*). A right tibia was also recovered from Spit No. 58A; it is shorter than the tibiae of LB1 and has been assigned as LB8 (*S9*). Four additional elements have been assigned to LB1 so far, all of which were recovered from surrounding Spits within Layer R.

3 Brief overview of carpal bone development

In humans, the primordial carpus is formed of skeletal blastema, a condensation of mesenchymal cells that migrate to the site of future osteogenesis of the wrist (*S10*). This mesenchymal condensation appears around day 37 of embryonic development and begins to show signs of chondrification by day 48 (*S11–S13*). As the carpus becomes chondrified over the next few days, interzones appear in the areas where the carpals will articulate with one another; this is followed by complete cavitation (i.e., separation of the

chondrifying blastema into distinct carpal shapes), which occurs between the 9th and 11th weeks (*S11, S14–S18*).

At this early stage of development, three of the carpals have already originated "approximately in their definitive form and change neither their shape nor their location in the course of further development" (*S19*: 22). These include the trapezium, the trapezoid, and the capitate (*S19*). During this same period, the condensed interzone between the scaphoid and centrale, which originate as separate elements, slowly begins to chondrify (*S19*). By the end of the 11th week, there is typically no remaining trace of this division between these two elements and the scaphoid has achieved its basic adult form (*S19*).

Carpal ligament formation follows a similar sequence as the carpals. The carpal ligaments are derived from mesenchyme and begin to show their distinguishing characteristics by the 9th week (*S20*). By the end of the 14th week, organization of the carpal ligament complex is complete (*S20*).

Although ossification of the chondrified carpals is not complete until adolescence, their distinctive shapes, articulations, and ligamentous configurations are set by these early developmental processes before the fetus enters its second trimester (*S11, S14, S17, S19–S22*). In total, the developmental evidence indicates that the mechanisms for shape differentiation of the carpals occur early in ontogeny (*S11, S14–S16, S18, S19, S21*). The majority of non-lethal pathologies and growth disorders do not begin to affect the skeleton until after initial carpal shape differentiation has occurred (*S23, S24*). This evidence reduces the likelihood that a specific pathology or growth disorder could result in an adult modern human with an otherwise normal primitive hominin wrist.

4 3D shape quantitative analyses

Tables S4A, B, and C provide a list of the variables that best account for the variation observed along the canonical axes of each analysis (Figs. 1–3). CAN1 best reflects the major shape differences between the primitive and derived carpal conditions in these hominids. The means, standard deviations, and individual/fossil values for the variables that drive CAN1 in each analysis are shown in Table S5. In the multivariate analyses all fossil specimens, along with the two modern humans with pituitary disorders, were analyzed as test classification cases only. In other words, these specimens do not contribute to any of the observed variation along the canonical axes. However, assignment of these specimens to their own respective *a priori* groups results in essentially identical plots.

In each analysis, Upper Paleolithic *H. sapiens* and Neandertals, as well as the two modern humans with pituitary disorders (note that no capitate from the pituitary dwarf was preserved), cluster along CAN1 with modern humans because they share the derived morphological characteristics of the wrist (Figs. 1–3). In contrast, *H. floresiensis* clusters along CAN1 with the great apes because they all share primitive carpal shape characteristics (Figs. 1–3).

The results of the discriminant function analyses are summarized in Tables S6–S11. The cross-validated posterior probabilities of correctly classifying each carpal to the extant genus to which it belongs are shown in Tables S6, S8, and S10 while the classification results for the test cases (i.e., all fossil specimens and the two modern humans with pituitary disorders) are shown in Tables S7, S9, and S11. Since the test cases include specimens not included in the construction of the discriminant model, the

probabilistic assessments of genus membership for such specimens are used for heuristic purposes only to demonstrate morphological affinities. Of the 247 modern human carpals analyzed, only 11 are misclassified incorrectly (4.5%); of the 292 nonhuman primate carpals analyzed, only 5 are misclassified as modern human (1.7%). Fifteen of the sixteen misclassifications occur with the scaphoid (Table S8), which, of these three carpal bones, is the most similar between modern humans and African apes. Overall, the discriminant results testify to the major shape differences between the primitive and derived carpal conditions in these primates.

The cross-validation procedure of the discriminant analysis for the trapezoid resulted in the correct classification of 111 *Homo* (100%), 42 *Pan* (89%), 42 *Gorilla* (96%), 16 *Pongo* (80%), and 19 *Papio* (100%; Table S5). All the test cases are classified as *Homo* except for LB1, which is classified as *Pongo* (Table S7). These results indicate that the shape of the trapezoid in modern humans and Neandertals is derived in comparison to the primitive hominid condition seen in great apes and LB1.

The classification of the LB1 trapezoid as belonging to *Pongo* rather than *Pan* or *Gorilla* in this analysis is not surprising. *Pongo* and *Pan* cluster together along CAN1 and CAN2 (Figs. 1 and 3) and are most often misclassified as one another (Tables S6 and S10) because they share primitive trapezoid and capitate features (*Gorilla* is uniquely derived in having lost the articulation between the trapezoid and capitate). However, the 2nd metacarpal articulations in the *Pongo* trapezoid (as well as in LB1) slant more strongly in a proximal direction than in *Pan* (Fig. 1, bottom row). This results in differences between *Pan* and *Pongo* in the angles between the trapezium and 2nd metacarpal surfaces (Table S4A) and explains why the LB1 trapezoid shows a stronger

affinity to *Pongo*. However, both the scaphoid (which has a congenitally-fused centrale) and capitate of LB1 are more African ape-like (Figs. 2 and 3), and no remains of extant or fossil orangutans have ever been recovered on Flores Island.

The cross-validation procedure of the discriminant analysis for the scaphoid resulted in the correct classification of 106 *Homo* (91%), 36 *Pan* (75%), and 37 *Gorilla* (77%; Table S8). Only *Homo*, *Pan*, and *Gorilla* were included in this analysis because these three genera have a congenitally fused scaphoid and centrale (a derived condition among hominids). Both the OH7 and LB1 scaphoids are classified as *Pan*, while the remaining test cases are all classified as *Homo* (Table S9). In Figure 2, the scaphoids of Shanidar 3 and the modern human pituitary giant cluster along the edge of the observed variation in modern *Homo* that is closest to the African ape clusters; this is also reflected in their posterior probabilities of genus membership (Table S9). Along CAN1, specimens of modern *Homo* that fall closest to the African ape cluster tend to have a more distally-closed capitate joint surface, which results in a narrower angle between the capitate and trapezium-trapezoid joint surfaces; the scaphoids of Shanidar 3 and the modern human pituitary giant are similar in this respect. However, both clearly resemble the scaphoids of *Homo* overall.

The cross-validation procedure of the discriminant analysis for the capitate resulted in the correct classification of 19 *Homo* (100%), 15 *Pan* (68%), 24 *Gorilla* (100%), and 15 *Pongo* (75%; Table S10). The test classification results are as follows: the LB1 and AL288-1w (*A. afarensis*, 'Lucy') capitates are classified as *Pan*; TM1526 (*A. africanus*) is classified as *Pongo*; AL333-80 (*A. afarensis*) is classified as *Homo*; the capitates of the pituitary giant, Amud 1, and Krapina are classified as *Homo*; and the La

Chapelle-aux-Saints capitate is classified as *Pongo* (Table S11). The La Chapelle capitate is the only specimen in all of the analyses for which the posterior probability results do not reasonably correspond with the canonical variates plots. Along CAN1, this capitate is intermediate among the three Neandertal capitates, which all clearly cluster with modern humans (Fig. 3). Canonical variates analysis differs from discriminant function analysis in that the former reduces the multidimensional variation into dimensions equal to the number of *a priori* groups minus one, while the latter is based on dimensions equal to the number of predictor variables (p) used. In general, the La Chapelle capitate is intermediate between the genus means for *Homo* and *Pongo* with respect to the capitate measurements analyzed. Therefore, in the p-dimensional space of the discriminant analysis the La Chapelle capitate occupies a space that is in between the respective centroids for *Homo* and *Pongo* but closer to the latter. This effect disappears when the p-dimensional space is reduced into the three dimensions of the canonical analysis (Fig. 3). In this case, the canonical analysis better captures the morphological affinities of this particular capitate, which resembles modern human and Neandertal capitates rather than those of great apes, *Australopithecus*, and LB1.

5 Additional descriptions of LB1's scaphoid and capitate

The distinguishing characteristics of LB1's trapezoid were discussed in the main text and are not repeated here. Instead, we provide additional descriptions of its scaphoid and capitate, both of which show distinct morphology that is comparable to that of its primitively shaped trapezoid.

The LB1 scaphoid is most similar to that of *Pan*, *Gorilla*, and OH7 (*H. habilis*). Its primitive hominin characteristics include (i) a fused centrale (Fig. 2); (ii) an

articulation for the capitate that is distally more closed (Fig. 2, middle and bottom rows); (iii) a less robust palmar tubercle (Fig. 2); and (iv), its trapezium-trapezoid articulation does not extend out onto the scaphoid tubercle (Fig. 2, middle row). The scaphoids of modern humans and Neandertals differ from the primitive hominin condition in having (i) an articulation for the capitate that is distally more open (Fig. 2, middle and bottom rows) (*S1*); (ii) a more robust palmar tubercle (Fig. 2) (*S1, S25*); and (iii), a trapezium-trapezoid articulation that extends out onto the scaphoid tubercle (Fig. 2, middle row) (*S1, S25*).

The LB1 capitate is most similar to that of *Pan* and AL288-1w (*A. afarensis*). Its primitive hominid characteristics include (i) the dorsal aspect of the scaphoid articular surface extends distally along the radial side of the neck (Fig. 3, middle row); (ii) a relatively small articulation for the trapezoid that occurs more dorsally on the disto-radial side (Fig. 3, middle row); (iii) a restricted or waisted capitate neck (Fig. 3, top row) (*S26, S27*); and (iv) a more radially-oriented second metacarpal articulation (Fig. 3, top row) (*S26–S30*). Modern human and Neandertal capitates differ from the primitive hominid condition in having (i) a scaphoid articulation that does not typically extend distally onto the dorso-radial side of the neck; (ii) a relatively larger and more palmarly positioned trapezoid articulation (*S26, S27*); (iii) an expanded neck, particularly on the radial side (*S26, S27*); and (iv) a reduced relative area of the third metacarpal articulation with a beveling of the dorso-radial corner of that articulation to accommodate the third metacarpal styloid process (*S27, S31*).

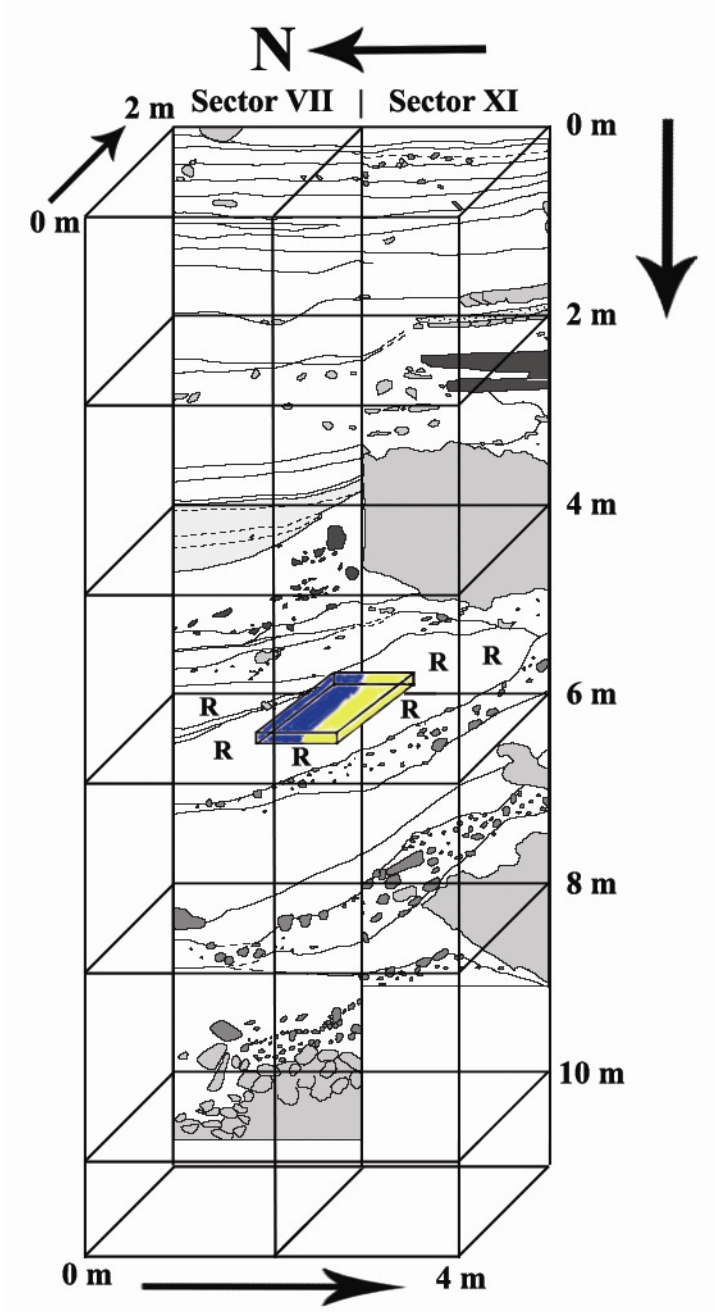

Fig. S1. The 2003 excavation of Sector VII resulted in the recovery of the cranium, mandible, and associated postcranial material of LB1 including the wrist bones (blue area). Subsequent excavation in 2004 of Sector XI resulted in the recovery of additional upper and lower limb elements (yellow area). The blue and yellow areas represent portions of Spit Nos. 59 and 58 within each respective sector; both areas occur within the same layer of clayey silt (Layer R) (see *S8* and *S9* for more stratigraphic details).

Table S1: Breakdown of the total wrist bone sample by extant genus and fossil specimen.

	Bone			
Extant genus	TZD	SCA	CAP	TOTAL
Homo	113	119	20	252
Pan	47	48	22	117
Gorilla	44	48	24	116
Pongo	20		20	40
Papio	19			19
Upper Paleolithic *H. sapiens*				
Qafzeh 9	1	1		2
Combe-Capelle 1	1	1		2
Neandertal				
Kebara 2	1	1		2
La Ferrassie 1	1	1		2
Amud 1	1		1	2
Regourdou 1		1		1
Regourdou 2		1		1
Shanidar 3		1		1
Shanidar 4		1		1
Shanidar 8		1		1
La Chapelle-aux-Saints			1	1
Krapina			1	1
H. habilis				
OH7		1		1
A. afarensis				
AL288-1w			1	1
AL333-40			1	1
A. africanus				
TM1526			1	1
H. floresiensis				
LB1	1	1	1	3
TOTAL	249	226	93	568

[1] TZD, trapezoid; SCA, scaphoid; CAP, capitate.

Table S2: Breakdown of the modern human sample by recent geographical origin.

	Bone			
Recent Geographical Origin	TZD	SCA	CAP	TOTAL
African	34	34	1	69
American	17[2]	19[2]	10	46
Asian	22	26		48
Australian	9	9	6	24
European	31[3]	31[3]	3[3]	65
TOTAL	113	119	20	252

[1] TZD, trapezoid; SCA, scaphoid; CAP, capitate

[2] includes one bone from an individual with pituitary dwarfism

[3] includes one bone from an individual with pituitary giantism

Table S3. Hominin remains attributed to LB1, excavated from the Late Pleistocene levels of the Sector VII/XI trench at Liang Bua in 2003 and 2004 (bones analyzed in this study shown in bold).

Sector	Spit No.	Designation	Element	Sector	Spit No.	Designation	Element
VII	59	LB1/1	cranium	VII	59	LB1/31	metatarsal III, right
VII	59	LB1/2	mandible	VII	59	LB1/32	metatarsal IV, right
VII	59	LB1/3	atlas	VII	59	LB1/33	metatarsal V, right
VII	59	LB1/4	costal fragments	VII	59	LB1/34	pedal phalanx, proximal
VII	59	LB1/5	clavicle, right	VII	59	LB1/35	pedal phalanx, proximal
VII	59	LB1/6	ribs	VII	59	LB1/36	pedal phalanx, proximal
VII	59	LB1/7	innominate, right	VII	59	LB1/37	pedal phalanx, proximal
VII	59	LB1/8	femur, right	VII	59	LB1/38	pedal phalanx, proximal
VII	59	LB1/9	femur, left	VII	59	LB1/39	pedal phalanx, middle
VII	59	LB1/10	patella, left	VII	59	LB1/40	manual phalanx, middle
VII	59	LB1/11	patella, right	VII	59	LB1/41	pedal phalanx, proximal
VII	59	LB1/12	tibia, left	VII	59	LB1/42	manual phalanx, middle
VII	59	LB1/13	tibia, right	VII	59	LB1/43	pedal phalanx, distal
VII	59	LB1/14	fibula, right	VII	59	**LB1/44**	**scaphoid, left**
VII	59	LB1/15	talus, left	VII	59	**LB1/45**	**capitate, left**
VII	59	LB1/16	navicular, left	VII	59	LB1/46[1]	hamate, left
VII	59	LB1/17	cuboid, left	VII	59	**LB1/47**	**trapezoid, left**
VII	59	LB1/18	ectocuneiform, left	VII	59	LB1/48	manual phalanx, middle
VII	59	LB1/19	mesocuneiform, left	VII	59	LB1/49	manual phalanx, distal
VII	59	LB1/20	entocuneiform, left	XI	58A	LB1/50	humerus, right
VII	59	LB1/21	metatarsal I, left	XI	58A	LB1/51	ulna, left
VII	59	LB1/22	metatarsal II, left	XI	58A	LB1/52	ulna, right
VII	59	LB1/23	metatarsal III, left	XI	58A	LB1/53	fibula, left
VII	59	LB1/24	metatarsal IV, left	XI	58A	LB1/54	talus, right
VII	59	LB1/25	metatarsal V, left	VII	62	LB1/55	manual phalanx, distal
VII	59	LB1/26	navicular, right	VII	59	LB1/56	pedal phalanx, middle
VII	59	LB1/27	cuboid, right	VII	59	LB1/57	pedal phalanx, distal
VII	59	LB1/28	ectocuneiform, right	XI	57A	LB1/58	phalanx
VII	59	LB1/29	metatarsal I, right	VII	59	LB1/59	metacarpal
VII	59	LB1/30	metatarsal II, right				

[1] Note the hamate is incomplete and thus was not included in this study

Table S4A: Correlations between each trapezoid variable and canonical axis (bolded values indicate the variables that best explain the observed variation along each axis).

Trapezoid				
Angle between the articular facets for		CAN1	CAN2	CAN3
2nd metacarpal (radial side)	2nd metacarpal (ulnar side)	0.00	0.09	0.13
2nd metacarpal (radial side)	scaphoid	0.18	-0.06	0.27
2nd metacarpal (radial side)	trapezium	0.08	-0.25	**0.44**
2nd metacarpal (ulnar side)	scaphoid	**0.51**	-0.22	-0.28
2nd metacarpal (ulnar side)	trapezium	0.14	-0.19	**0.63**
scaphoid	trapezium	-0.12	0.22	0.04
Relative surface area				
nonarticular		-0.13	**0.49**	0.12
2nd metacarpal (radial side)		-0.04	-0.14	-0.12
2nd metacarpal (ulnar side)		0.22	0.08	**0.35**
scaphoid		**0.44**	0.00	-0.28
trapezium		-0.03	**-0.37**	-0.23

Table S4B: Correlations between each scaphoid variable and canonical axis (bolded values indicate the variables that best explain the observed variation along each axis).

Scaphoid			
Angle between the articular facets for		CAN1	CAN2
capitate	radius	0.04	0.32
capitate	trapezium-trapezoid	**0.58**	**-0.34**
radius	trapezium-trapezoid	-0.24	0.02
Relative surface area			
capitate		0.29	**0.84**
radius		0.13	0.32
trapezium-trapezoid		**0.41**	0.19
nonarticular		**-0.34**	**-0.59**

Table S4C: Correlations between each capitate variable and canonical axis (bolded values indicate the variables that best explain the observed variation along each axis).

Capitate				
Angle between the articular facets for		CAN1	CAN2	CAN3
hamate	2nd metacarpal	0.26	-0.07	**-0.84**
hamate	3rd metacarpal	-0.22	**0.57**	-0.27
2nd metacarpal	3rd metacarpal	**0.37**	**-0.40**	**-0.56**
Relative surface area				
hamate		-0.01	0.12	0.42
2nd metacarpal		**0.35**	-0.11	-0.02
3rd metacarpal		**-0.45**	-0.09	**0.41**
scaphoid-lunate		-0.15	**-0.36**	0.32
trapezoid		**0.58**	0.27	**0.38**

Table S5: The means, standard deviations, and individual/fossil values for the variables that best account for the variation observed along the first axis of each canonical variates analysis.

	Variable																	
	Trapezoid[1]				Scaphoid[2]						Capitate[3]							
	mc2u-sca		r-sca		cap-tpmtzd		r-tpmtzd		r-na		mc2-mc3		r-mc2		r-mc3		r-tzd	
Extant genus	Mean	SD	Mean	SD	Mean	SD	Mean	SD	Mean	SD	Mean	SD	Mean	SD	Mean	SD	Mean	SD
Homo	38	10	8.3	2.4	82	8	14.6	1.9	44.0	4.2	142	8	4.8	1.0	10.1	1.0	3.7	1.4
Pan	69	6	14.3	1.5	67	5	12.9	1.3	45.8	3.4	100	9	3.1	0.8	13.1	1.0	1.9	0.5
Gorilla	61	8	14.1	1.9	70	7	12.1	1.8	50.2	4.3	98	9	2.3	0.7	14.8	1.2	0.0	0.0
Pongo	63	6	13.2	2.3							100	25	3.0	0.9	12.5	1.5	1.9	0.4
Papio	72	7	16.3	2.0														
Pituitary Disorders																		
dwarfism	34		4.9		92		16.0		39.2									
giantism	41		12.7		78		15.8		39.5		144		3.5		9.6		3.5	
U.P. *H. sapiens*																		
Qafzeh 9	39		11.2		73		16.4		37.9									
Combe-Capelle 1	34		5.6		93		14.8		42.2									
Neandertal																		
Kebara 2	31		13.7		81		17.9		40.5									
La Ferrassie 1	38		12.3		83		12.2		45.8									
Amud 1	34		6.1								126		5.8		7.2		2.5	
Regourdou 1					80		15.7		40.4									
Regourdou 2					77		15.2		41.4									
Shanidar 3					73		14.4		44.8									
Shanidar 4					66		15.2		47.3									
Shanidar 8					78		15.4		42.1									
La Chapelle											123		4.3		9.1		2.5	
Krapina											141		4.9		9.3		1.4	
H. habilis																		
OH7					58		10.4		49.3									
A. afarensis																		
AL288-1w											118		4.0		10.9		2.1	
AL333-40											133		6.3		11.5		1.8	
A. africanus																		
TM1526											128		4.3		11.6		2.0	
H. floresiensis																		
LB1	72		8.5		75		9.2		50.9		117		3.3		14.1		1.5	

[1] Trapezoid variables: mc2u-sca, angle between 2nd metacarpal (ulnar side) and scaphoid surfaces; r-sca, relative scaphoid area

[2] Scaphoid variables: cap-tpmtzd, angle between capitate and trapezium-trapezoid surfaces; r-tpmtzd, relative trapezium-trapezoid area; r-na, relative nonarticular area

[3] Capitate variables: mc2-mc3 angle between 2nd and 3rd metacarpal surfaces; r-mc2, relative 2nd metacarpal area; r-mc3, relative 3rd metacarpal area; r-tzd, relative trapezoid area

Table S6: The cross-validated posterior probabilities of correctly classifying each trapezoid to the extant genus to which it belongs.

	Homo	*Pan*	*Gorilla*	*Pongo*	*Papio*
Homo	**111**	0	0	0	0
%	**100.0**	0.0	0.0	0.0	0.0
Pan	0	**42**	0	3	2
%	0.0	**89.4**	0.0	6.4	4.3
Gorilla	0	1	**42**	1	0
%	0.0	2.3	**95.5**	2.3	0.0
Pongo	0	3	0	**16**	1
%	0.0	15.0	0.0	**80.0**	5.0
Papio	0	0	0	0	**19**
%	0.0	0.0	0.0	0.0	**100.0**

Table S7: The morphological affinity of each 'test' trapezoid based on the probabilities of extant genus membership.

Specimen Identification		*Homo*	*Pan*	*Gorilla*	*Pongo*	*Papio*
Pituitary Dwarf	modern human	**100**[1]	0	0	0	0
Pituitary Giant	modern human	**100**	0	0	0	0
Qafzeh 9	U.P. human[2]	**100**	0	0	0	0
Combe-Capelle 1	U.P. human	**100**	0	0	0	0
Kebara 2	Neandertal	**100**	0	0	0	0
La Ferrassie 1	Neandertal	**100**	0	0	0	0
Amud 1	Neandertal	**100**	0	0	0	0
LB1	*H. floresiensis*	0	0	0	**100**	0

[1] the probability expressed as a percentage (%)

[2] U.P., Upper Paleolithic

Table S8: The cross-validated posterior probabilities of correctly classifying each scaphoid to the extant genus to which it belongs.

	Homo	*Pan*	*Gorilla*
Homo	**106**	7	4
%	**90.6**	6.0	3.4
Pan	2	**36**	10
%	4.2	**75.0**	20.8
Gorilla	2	9	**37**
%	4.2	18.8	**77.1**

Table S9: The morphological affinity of each 'test' scaphoid based on the probabilities of extant genus membership.

Specimen Identification		*Homo*	*Pan*	*Gorilla*
Pituitary Dwarf	modern human	**100**[1]	0	0
Pituitary Giant	modern human	**64**	19	18
Qafzeh 9	U.P. human[2]	**93**	7	0
Combe-Capelle 1	U.P. human	**100**	0	0
Kebara 2	Neandertal	**100**	0	0
La Ferrassie 1	Neandertal	**99**	1	0
Regourdou 1	Neandertal	**98**	1	0
Regourdou 2	Neandertal	**100**	0	0
Shanidar 3	Neandertal	**55**	38	7
Shanidar 4	Neandertal	**88**	12	0
Shanidar 8	Neandertal	**99**	1	0
OH7	*H. habilis*	0	**99**	1
LB1	*H. floresiensis*	2	**89**	9

[1] the probability expressed as a percentage (%)

[2] U.P., Upper Paleolithic

Table S10: The cross-validated posterior probabilities of correctly classifying each capitate to the extant genus to which it belongs.

	Homo	*Pan*	*Gorilla*	*Pongo*
Homo	**19**	0	0	0
%	**100.0**	0.0	0.0	0.0
Pan	0	**15**	0	7
%	0.0	**68.2**	0.0	31.8
Gorilla	0	0	**24**	0
%	0.0	0.0	**100.0**	0.0
Pongo	1	4	0	**15**
%	5.0	20.0	0.0	**75.0**

Table S11: The morphological affinity of each 'test' capitate based on the probabilities of extant genus membership.

Specimen Identification		*Homo*	*Pan*	*Gorilla*	*Pongo*
Pituitary Giant[1]	modern human	**100**[2]	0	0	0
Amud 1	Neandertal	**100**	0	0	0
La Chapelle	Neandertal	18	1	0	**80**
Krapina	Neandertal	**99**	1	0	1
AL288-1w	*A. afarensis*	1	**84**	0	15
AL333-40	*A. afarensis*	**90**	5	0	4
TM1526	*A. africanus*	0	11	0	**89**
LB1	*H. floresiensis*	0	**72**	0	28

[1] neither capitate was available for analysis from the modern human pituitary dwarf

[2] the probability expressed as a percentage (%)

References

S1. M. W. Tocheri, Ph. D. Thesis, Arizona State University, Tempe, Arizona (2007).

S2. M. W. Tocheri, A. Razdan, R. C. Williams, M. W. Marzke, *J Hum Evol* **49**, 570 (2005).

S3. M. W. Tocheri, M. W. Marzke, D. Liu, M. Bae, G. P. Jones, R. C. Williams, A. Razdan, *Am J Phys Anthropol* **122,** 101 (2003).

S4. W. L. Jungers, A. B. Falsetti, C. E. Wall, *Yearb Phys Anthrop* **38,** 137 (1995).

S5. J. E. Mosimann, F. C. James, *Evol* **33,** 444 (1979).

S6. R. A. Johnson, D. W. Wichern, *Applied multivariate statistical analysis, 5th edition*

(Prentice-Hall, Inc., Upper Saddle River, NJ, 2002).

S7. P. Brown, T. Sutikna, M. J. Morwood, R. P. Soejono, Jatmiko, E. Wayhu Saptomo, Rokus Awe Due, *Nature* **431,** 1055 (2004).

S8. M. J. Morwood, R. P. Soejono, R. G. Roberts, T. Sutikna, C. S. M. Turney, K. E. Westaway, W. J. Rink, J. -x. Zhao, G. D. van den Bergh, Rokus Awe Due, D. R. Hobbs, M. W. Moore, M. I. Bird, L. K. Fifield, *Nature* **431,** 1087 (2004).

S9. M. J. Morwood, P. Brown, Jatmiko, T. Sutikna, E. Wayhu Saptomo, K. E. Westaway, Rokus Awe Due, R. G. Roberts, T. Maeda, S. Wasisto, T. Djubiantono, *Nature* **437,** 1012 (2005).

S10. B. K. Hall, *Amer Science* **76,** 174 (1988).

S11. R. O'Rahilly, D. J. Gray, E. Gardner, *Contributions to Embryology* **36,** 183 (1957).

S12. H. D. Senior, *Anat Rec* **42,** 35 (1929).

S13. G. L. Streeter, *Contributions to Embryology* **32,** 133 (1948).

S14. D. J. Gray, E. Gardner, R. O'Rahilly, *Am J Anat* **101,** 169 (1957).

S15. R. O'Rahilly, *Anat Rec* **103,** 187 (1949).

S16. R. O'Rahilly, E. Gardner, *Anat Embryol* **148,** 1 (1975).

S17. L. Scheuer, S. Black, *Developmental Juvenile Osteology* (Academic Press, London, UK, 2000).

S18. J. Whillis, *J Anat* **74,** 277 (1940).

S19. R. Čihák, *Ergebnisse der Anatomie und Entwicklungsgeschichte* **46**, 1 (1972).

S20. J. A. Mérida-Velasco, J. D. Garcia-Garcia, J. Espín-Ferra, I. Sánchez-Montesinos, *Anat Rec* **245,** 114 (1996).

S21. S. Durand, V. Delmas, M. -C. Ho Ba Tho, Z. Batchvarova, J. F. Uhl, C. Oberlin,

Surg Radiol Anat **28,** 355 (2006).

S22. B. Tardif, F. Duparc, J. M. Muller, P. Freger, *Chir Main* **17,** 266 (1998).

S23. J. W. Spranger, P. W. Brill, A. K. Poznanski, *Bone Dysplasias: An Atlas of Genetic Disorders of Skeletal Development, 2nd ed.* (Oxford University Press, Oxford, England, 2002).

S24. E. Zelzer, B. R. Olsen, *Nature* **423,** 343 (2003).

S25. R. L. Susman, N. Creel, *Am J Phys Anthropol* **51,** 311 (1979).

S26. O. J. Lewis, *Functional Morphology of the Evolving Hand and Foot* (Clarendon Press, Oxford, UK, 1989).

S27. H. M. McHenry, *Am J Phys Anthropol* **62,** 187 (1983).

S28. M. W. Marzke, *J Hum Evol* **12,** 197 (1983).

S29. M. W. Marzke, *Am J Phys Anthropol* **102,** 91 (1997).

S30. C. V. Ward, M. G. Leakey, A. Walker, *Evol Anthropol* **7,** 197 (1999).

S31. M. W. Marzke, R. F. Marzke, *Am J Phys Anthropol* **73,** 415 (1987).